Available online at www.sciencedirect.com
ScienceDirect
Earth and Planetary Science Letters 264 (2007) 89 – 103
EPSL
www.elsevier.com/locate/epsl

Micrometer-scale cavities in fibrous and cloudy diamonds — A glance into diamond dissolution events

Ofra Klein-BenDavid [a,*], Richard Wirth [b], Oded Navon [c]

[a] *Department of Earth Sciences, Durham University, Science Labs, Durham, DH1 3LE, UK*
[b] *GeoForschungsZentrum, Potsdam, Telegrafenberg, Div.4, D-14473, Potsdam, Germany*
[c] *Institute of Earth Sciences, The Hebrew University of Jerusalem, Jerusalem 91904, Israel*

Received 17 July 2007; received in revised form 5 September 2007; accepted 11 September 2007
Available online 15 September 2007
Editor: R.W. Carlson

Abstract

Micrometer sized internal cavities in diamonds preserve evidence of diamond dissolution events. Combining the methods of focused ion beam (FIB) sample preparation and transmission electron microscopy (TEM) enables these features to be studied in detail.

Micrometer-scale cavities are found in the inner parts of fibrous and cloudy kimberlitic diamonds. Their filling consists of amorphous matrix, secondary nano-crystals, volatiles and in some cases larger resorbed crystals. Trapped minerals include corundum, Kappa-alumina, quartz, olivine, moissanite-6H and Ca–Mg carbonates. This is the first observation of Kappa-alumina in nature. Secondary nano-minerals are observed within the amorphous matrix and include carbonates, Al-oxide, fluorite, ilmenite and secondary diamond crystals. The amorphous matrix is spongy and its composition is dominated by amorphous carbon, nitrogen, chlorine and also contains water. When no crystalline phases are observed, the matrix is also enriched in alumina, silica and in some cases calcium.

We propose that micrometer scale cavities in diamonds form during dissolution events induced by the introduction of oxidizing hydrous fluids into the diamond growth area. Hydrous fluids are the main dissolving agents for most kimberlitic diamonds [Fedortchouk, Y., Canil, D., Semenets, E., 2007. Mechanisms of diamond oxidation and their bearing on the fluid composition in kimberlite magmas. Am. Mineral. 92, 1200–1212]. At diamond forming conditions silica and alumina are enriched in hydrous fluids that are in equilibrium with eclogites [Kessel, R., Ulmer, P., Pettke, T., Schmidt, M.W., Thompson, A.B., 2005. The water-basalt system at 4 to 6 GPa: Phase relations and second critical endpoint in a K-free eclogite at 700 to 1400 °C. Earth Planet. Sci. Lett. 237, 873–892]; this is consistent with the increased solubility of alumina with increased pressure and temperature in the Na–Cl bearing fluids [Manning, C.E., 2006. Mobilizing aluminum in crustal and mantle fluids. J. Geochem. Explor. 89, 251–253; Manning, C.E., 2007. Solubility of corundum+kyanite in H2O at 700C and 10 kbar: evidence for Al–Si complexing at high pressure and temperature. Geofluids. 7, 258–269]. Additionally, hydrous fluids may leach grain boundaries that are enriched in alumina in peridotitic environments [Hiraga, T., Anderson, I.M., Kohlstedt, D.L., 2004. Grain boundaries as reservoirs of incompatible elements in the Earth's mantle. Nature. 427, 699–703; Wirth, R., 1996. Thin amorphous films (1–2 nm) at olivine grain boundaries in mantle xenoliths from San Carlos, Arizona. Contrib. Mineral. Petrol. 124, 44–54].

Diamond dissolution will form oxidized carbon species and may decrease the solubility of silica and alumina in the dissolving agent leading to their precipitation.

* Corresponding author.
E-mail address: o.k.bendavid@durham.ac.uk (O. Klein-BenDavid).

0012-821X/$ - see front matter
doi:10.1016/j.epsl.2007.09.004

Diamond forming fluids that are trapped in sub-micrometer inclusions in the same fibrous diamonds are the dominant fluid component in the diamond growth area. Corrosive hydrous fluids are less common and appear as short, discrete events, followed by the return of the common diamond forming fluids and continued diamond precipitation.

Keywords: dissolution cavities; amorphous matrix; hydrous fluids; Al-rich assemblages; kappa-alumina; moissanite

1. Introduction

Diamond dissolution at mantle conditions is indicated by changes in diamond morphology and the formation of etch pits. Dissolution patterns followed by additional diamond growth are observed in cathodoluminescence (CL) images of many diamonds (Bulanova, 1995; Schulze et al., 2003). Etched, cavity-rich zones followed by subsequent fibrous growth have also been observed in a coated diamond from Canada (Klein-BenDavid et al., 2004). During dissolution, diamond morphology changes from a sharp octahedron through combinations of octahedron and hexoctahedral forms to spherical hexoctahedral with rounded faces (Khokhryakov and Pal'yanov, 2007). Etching creates negatively oriented triangular pits (trigons) on the octahedral faces of the diamond and square pyramidal pits on the cubic faces. All pits grow larger and deeper as dissolution proceeds (Robinson, 1978; Sunagawa, 1984; Robinson et al., 1989; McCallum et al., 1994; Kozai and Arima, 2005).

Diamond dissolution depends on the redox condition, the temperature of the host magma (Arima, 1998) and the H_2O content of the system (Kanda et al., 1977; Pal'yanov et al., 1995; Khokhryakov et al., 2001, 2002). Diamond volume-loss and the degree of etching were also found to increase with increasing temperature and oxygen fugacity (Fedortchouk et al., 2005). Kimberlites are thought to be the main medium in which diamonds corrode (Robinson et al., 1989), and diamond dissolution rates in kimberlitic fluids are as high as 0.12 mm/h at hot oxidizing conditions such as 1300 °C at HM buffer; (Kozai and Arima, 2005). Fedortchouk et al. (2007) have shown that diamond oxidation rate is the same in the kimberlitic melts with a free fluid phase and in a pure H_2O or CO_2 fluid, suggesting that the process of diamond oxidation is its reaction with the fluid and not with the melt.

Fibrous diamonds are precipitated under high carbon super-saturation conditions that accelerate growth and lead to high N abundance, fibril structure and the entrapment of numerous sub-micrometer inclusions (Sunagawa, 1984, 1990). The nitrogen in fibrous diamonds typically has a low aggregation state (a-centers) suggesting short mantle residence time. Attempts to estimate fibrous diamond age have indeed yielded ages similar to that of the host kimberlite (Pearson et al., 1998; Burgess et al., 2002). Old fibrous diamonds may have existed initially; however, their imperfect crystal structure and high impurity content made them more sensitive to dissolution and material loss to more perfect diamonds.

Internal clouds of microinclusions within octahedral diamonds typically lack the fibril structure that is a characteristic of the fibrous stones; and also have higher nitrogen aggregation (a–b canters). Zedgenizov et al. (2006) have suggested that the fibrous structure may have existed initially, but have since undergone annealing during the octahedral growth period. Thus, the clouds grew at conditions similar to those of the fibrous diamonds and their microinclusions carry fluids of similar composition.

Pressures and temperatures estimates for microinclusions bearing diamonds range between conditions similar to those calculated for gem diamonds (cloudy diamonds, 1000–1200 °C, 4–6 GPa; Navon, 1991; Izraeli et al., 2004) to slightly lower equilibrium temperatures (fibrous coats, 930–1010±50 °C, 4.2 to 4.6 GPa; Tomlinson et al., 2006). Tomlinson et al. (2006) argue that the low temperature may account for the low degree of nitrogen aggregation.

Previous TEM studies of microinclusion bearing diamonds have shown abundant sub-micrometer inclusions which contain high-density fluids (HDF). The diamonds have crystallized from the same HDFs that they trapped and when they cooled, secondary minerals, such as carbonates, mica, quartz, halides and apatite were precipitated from the fluid, leaving residual volatile-rich, low-density fluid (Lang and Walmsley, 1983; Guthrie et al., 1991; Walmsley and Lang, 1992a,b; Klein-BenDavid et al., 2006). In some cases the material was not crystallized and solidified as amorphous material. The estimated bulk composition of the trapped phases is in accordance with the bulk composition of single microinclusions detected by electron probe micro analysis (EPMA) minus the residual low-density fluid (water+K_2O) that was lost during the

Table 1
Mineral and fluid composition of the studied diamond

Diamond	Habit	HDF composition	Included minerals	S–Ni–Fe inclusions	Paragenesis	Cavity filling
KFF-165 [a]	Cloudy diamond	Saline HDF	CPX, Carbonate		eclogitic	Amorphous matrix + kappa alumina + moisoniate 6H + nano fluorite crystal
UB 5–41 [b]	Fibrous cube	Mg-poor carbonatitic HDF	–	+	unknown	Amorphous matrix + carbonate crystals + corundum crystals + nano ilmenite crystal
UB 3105 [b]	Cloudy diamond	No HDF found	Mg–Fe silicate, Chromite	+	peridotitic	Amorphous matrix + carbonate crystals + corundum crystals + olivine + quartz
ON-DVK-294 [c]	Coated diamond	Saline and carbonatitic HDF	Cr-diopside, Chromite, Olivine		peridotitic	Amorphous matrix
CNG 2 [d]	Fibrous cube	Silicic HDF	–		unknown	Al-depleted amorphous matrix + nano diamond crystals

[a] (Izraeli et al., 2001, 2004).
[b] (Klein-BenDavid et al., 2003 and in Preparation; Logvinova et al., 2003).
[c] (Klein-BenDavid et al., 2004, 2007).
[d] (Klein-BenDavid, unpublished data).

preparation of the samples for TEM analyses (Klein-BenDavid et al., 2006).

Large cavities were also found in fibrous growth zones of two diamonds from Canada and Russia (Klein-BenDavid et al., 2006). These cavities are distinct from the sub-micron size microinclusions in their size, shape and composition. The cavities are a few micrometers in size, have anhedral edges and contain an amorphous matrix rich in Al, Si and Ca. The material is distributed heterogeneously in the cavity, with some areas rich in amorphous Al_2O_3, some in amorphous silica and some in amorphous $CaCO_3$.

Here we report the internal structure and mineralogy of five more cavities in inclusion-rich zones of fibrous, coated and cloudy diamonds. The cavities were found in both peridotitic and eclogitic diamonds carrying micro-inclusions of varying fluid composition and in a fluid-free diamond. The cavities were exposed in a polished

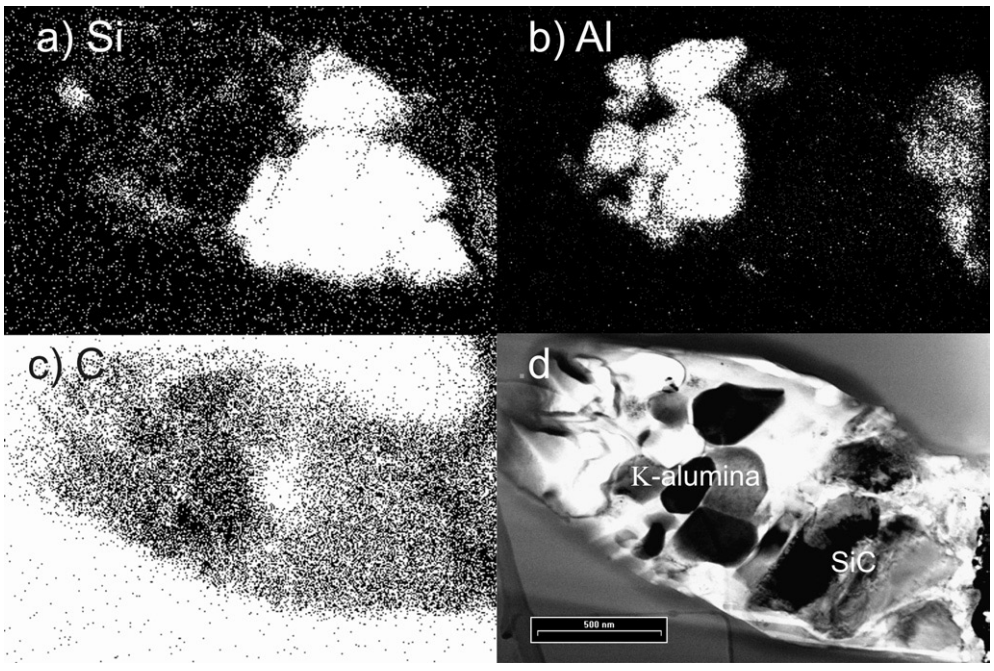

Fig. 1. Cavity in foil #710 in diamond KFF-165. (a–c): Si, Al and C EDX element maps, Si bearing phases are concentrated in the right part of the cavity, while Al_2O_3 is concentrated in the centre. The amorphous matrix is rich in carbon. (d) a TEM bright field (BF) image. The cavity is anhedral and its filling is highly heterogeneous in composition. The gray and black phases in the centre of the cavity are all κ-alumina and the corroded gray phases in the right of the cavity are moissanite-6H.

Table 2
Analyses of selected phases and matrix in the cavities

Diamond	UB 5–41					UB 5–41				UB 3105					
Foil	#731					#445				#543					
Description	Carbonte	Matrix&	Matrix	Matrix	Matrix	Matrix	Matrix	Matrix	Element map*	Olivine	Carbonte	Carbonte	corundom	Matrix	Matrix
Analysis no.	73109	73106	73108	73113	73114	14	12	18	EM	#543_R	#543_01	#543_06	#543_03	#543_04	#543_07
wt.%															
SiO_2		6.6	10.9	28.6	12.6	3.5	94.7	2.5	14.8	39.2				38.1	3.8
TiO_2									2.3						
Al_2O_3		43.5	38.5	16.5	71.2	93.5	5.3	7.0	69.1				100.0	16.0	9.8
FeO		6.1	41.5	3.1	2.8	1.6		1.6	1.9	6.5				5.0	2.6
MgO	39.2									54.3	36.9			7.8	3.0
CaO	60.8	15.2	3.1	14.3	3.8	0.9		88.2	9.8		63.1	100.0		11.5	66.7
BaO			1.9											8.8	
K_2O		5.5	2.4	11.1	2.6				1.1						0.8
P_2O_5		7.7		6.3	2.2										5.6
Cl		9.3	1.7	7.7	2.2	0.8		0.8	1.3					6.3	7.7
SO_3		6.2		12.5	2.5									6.5	
SrO															
Cr_2O_3															
NiO															

& sample analyses of the matrix of the cavity.
* over all composition of a large salected area within the cavity.
£ these compositions are given in element weight percent rather then oxides because of the dominance of non-oxide components (i.e. SiC, KCl).

diamond slab and do not extend to the diamond surface, suggesting that they were formed at the diamond stability field and were locked in the diamond during subsequent diamond growth.

2. Samples

Large cavities were found in seven foils extracted from five diamonds. Diamond KFF-165 originates from the Koffiefontein mine South-Africa; diamonds UB 5–41 and UB 3105 are from Yubileinaya mine, Russia; diamond CNG 2 is a placer diamond from Congo and diamond ON-DVK-294 is from the Diavik mine Canada. The cavities in diamond ON-DVK-294 and one of the cavities in diamond UB 5–41 were briefly described by Klein-BenDavid et al. (2006) and are discussed here together with the other cavities.

Diamonds KFF-165 and UB 3105 are cloudy diamonds and the cavities were found in the internal cloudy region. Diamonds UB 5–41 and CNG 2 are fibrous cubes. Diamond ON-DVK-294 is a coated diamond with an inclusion-free core and a complex fibrous coat. The size of the diamonds ranges between 2 and 4 mm, the fibrous and coated diamonds are gray to green in colour and the cloudy diamonds are transparent except for the dark internal cloud (Table 1).

EPMA analyses had revealed HDF-bearing micro-inclusions in four of these diamonds. Such microinclusions were also detected in the TEM images either in the same foil with the cavities or in neighbouring foils from the same diamond.

The composition of the HDF in the different diamonds varies. In diamonds KFF-165 and ON-DVK-294 they are intermediate between a saline and a carbonatitic end-member compositions with the letter being more carbonatitic (Izraeli et al., 2001; Klein-BenDavid et al., 2004, 2007); diamond UB 5–41 carries Mg-poor carbonatitic HDFs (Klein-BenDavid et al., in preparation) and diamond CNG 2 carries a silica-rich HDF (Klein-BenDavid et al., unpublished data). Eclogitic and peridotitic mineral microinclusions (<1 μm) were detected in three of the diamonds (see Table 1).

3. Methods

3.1. TEM analysis

3.1.1. Sample preparation

Ultra-thin diamond foils (~200 nm, see Supplementary data — (SP1)) were prepared using the focused ion beam (FIB) of a FIB2000 instrument at GFZ, Potsdam. Details of the FIB milling of diamond and TEM foil

UB 3105				ON-DVK-294				CNG 2			CNG 2		KFF-165		
#550				#450				#1143			#1143		#710		
Matrix	Matrix	Matrix	Matrix	Matrix	Matrix	Matrix	Element map*	Matrix	Matrix		Matrix[&]	Matrix	Matrix	Matrix	Element map*
#550_01	#550_02	#550_03	#550_07	48	37	47	EM	2	3		1	4	#71008	#71009	710_1EM
9.2	2.0	20.3	58.0	3.8	55.3	0.6	34.7	91.2	80.1	Si[£]		37.1	6.3	63.6	29.3
										Ti					
39.0	5.7	32.6	25.8	94.8	26.4	1.3	29.2		2.1	Al	4.6	13.8	84.3	3.8	69.0
14.2	1.6	13.8	2.6	0.5	7.6	0.6	6.9			Fe	2.7	3.6	1.6		0.5
						0.9	5.5			Mg	0.4	8.6			
5.4	84.8	4.5	2.9	0.6	6.7	94.4	15.8		0.6	Ca	9.6	2.4	2.4	11.4	0.6
										Ba					
7.7		6.9	2.1	0.3	1.8	1.0	2.5	6.7	14.6	K	52.8	14.1	3.4	18.2	0.6
	2.0				2.2		3.8			P					
2.3	1.4	2.9	1.1				0.3	2.8	3.4	Cl	29.9	11.4	0.3		
16.8	2.4	19.0	3.1				1.4			S		8.5	1.6	2.9	
						1.1				Sr					
										Cr					
5.3			1.4							Ni		0.4			

& sample analyses of the matrix of the cavity.
* over all composition of a large salected area within the cavity.
£ these compositions are given in element weight percent rather then oxides because of the dominance of non-oxide components (i.e. SiC, KCl).

preparation are given by Wirth (2004) and Klein-BenDavid et al. (2006).

3.1.2. Chemical analysis and electron diffraction

TEM analysis and imaging were conducted using a Philips CM200 microscope with a LaB6 electron source and a FEI Tecnai™ G2 F20 X-Twin microscope with a FEG electron source. The acceleration voltage was 200 kV in both microscopes. Electron energy-loss spectroscopy (EELS) was conducted using a Gatan imaging filter (GIF™). Foil thickness, necessary for absorption correction of the EDX spectra, was measured with EELS using the zero-loss spectrum and the total EEL spectrum (Egerton, 1996). The electron inelastic

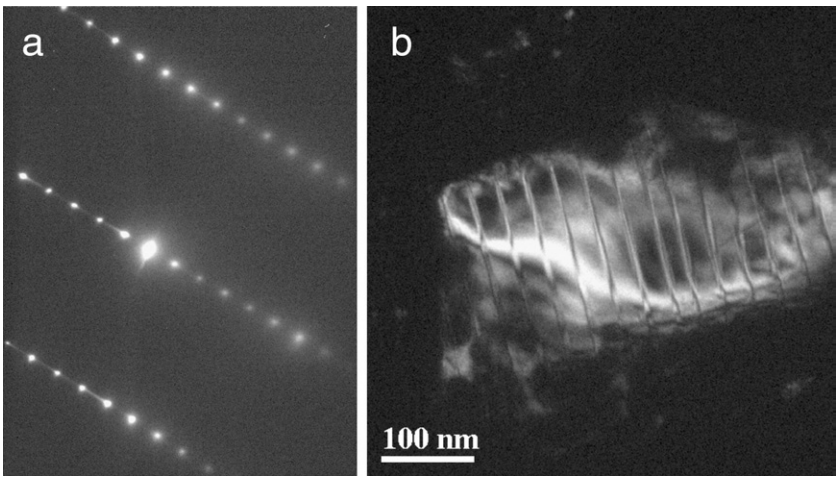

Fig. 2. Moissanite-6H crystals in the cavity of Fig. 1. (a) Diffraction pattern of the crystal. Streaking is observed in the pattern with (000l) reflections and reflects the superstructure. (b). TEM dark field (DF) image using the (0002) reflection, the crystal superstructure in pronounced in the image.

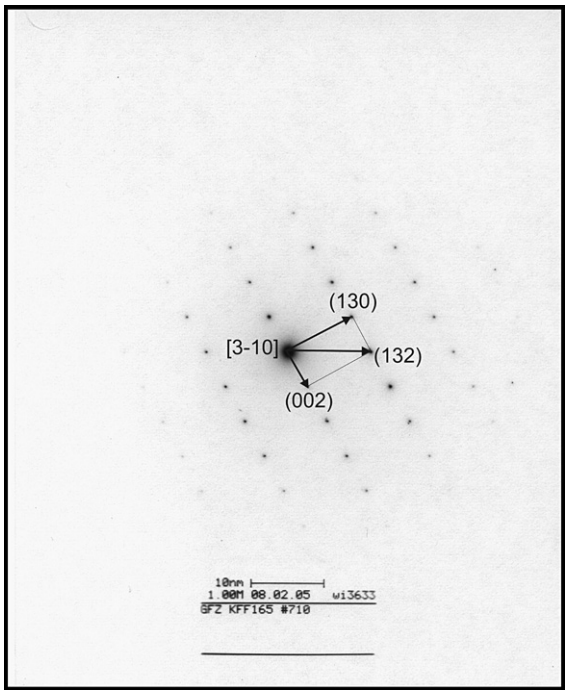

Fig. 3. Diffraction pattern of the κ-alumina of Fig. 1 with [3–10] zone axis, the diffraction indicates orthorhombic structure, d-spacings can be found in Table 3.

mean free path in diamond was calculated using the formalism given by Egerton (1996).

Chemical analysis was carried out using an energy dispersive X-ray spectrometer (EDAX). The details of the measurement conditions and the data reduction procedures are given in Klein-BenDavid et al. (2006). The total error estimated for major elements (concentrations >10 wt.%) is 2–5%, for minor elements (concentration 5–10 wt.%) it is 7–15% and for lower concentrations the error may exceed 50%. Sodium was not analyzed due to interference of its K_α peak with the Ga L_α peak.

It should be noted that in the TEM, phases that are stacked one on top of the other are analysed together, making it difficult to determine the accurate chemical composition of individual phases. Additionally, due to the large size of the cavities relative to foil thickness, some phases may be missed in the almost two dimensional cross sections of the cavities.

4. Results

4.1. Diamond foils description

4.1.1. Cavities in foil #710, Diamond KFF-165 (Koffiefontein, South Africa)

The cavity in this foil has an ellipsoidal shape (1×1.9 μm^2) with anhedral faces (Fig. 1). The cavity filling comprises both crystalline and amorphous phases.

Four fragments of moissanite-6H occupy the right hand side of the cavity (Fig. 1a and d) The EDX analysis of the fragments detects only Si and C (Table 2) and the diffraction patterns (Fig. 2a) indicate hexagonal symmetry. Streaking is observed in the diffraction pattern (light line between the diffraction points in Fig. 2a), and is the result of very small intercalated lamellae visible in the dark field image of Fig. 2b. The margins of the fragments are anhedral and the gaps between them are filled with amorphous matrix that is rich in Si and C (Fig. 2a,c), suggesting that they were once a single crystal that was resorbed (or amorphysized) in the cavity.

The grey and dark phases in the centre of the cavity (Fig. 1b, d) are composed of Al_2O_3. However, the diffraction data indicate that the phase is orthorhombic and does not fit the structure of corundum (Fig. 3). The spacing between planes (Table 3) are similar to those of κ-alumina,

Table 3
Diffraction data for phases included in the cavities and micro inclusions

Diffraction number	Diamond	Foil	Mineral	Dhkl observed	hkl
#3255	UB 3105	#543	Olivine	10.03	(010)
				4.27	(110)
#3256	UB 3105	#543	Olivine	3.9	(021)
				5.8	(001)
#3621	KFF-165	#710	Moissanite 6H	0.27	(10–11)
				0.258	(10–12)
				1.568	(0001)
#3625	KFF-165	#710	Moissanite 6H	0.155	(110) or (018)
				0.142	(109)
#3627	KFF-165	#710	Fluorite	0.197	(202)
				0.171	(311)
#3628	KFF-165	#710	Fluorite	0.314	(111)
#3637	UB 5–41	#731	Aragonite	3.8	(101)
				2.64	(102)
				5.58	(001)
#3636	UB 5–41	#731	Serpentine	0.74	(001) or (002)
#3633	KFF-165	#710	Kappa-alumina	2.42	130
				4.41	002
				2.12	132

Angels between plans

Diffraction number	Diamond	Foil	Mineral	Angels between plans	Observed	Calculated
#3633	KFF-165	#710	Kappa-alumina			
				<(130)/(132)	29°	28.28°
				<(132)/(002)	61°	61.72°

a phase known only as a synthetic variant, making this the first report of κ-alumina in a natural sample.

In addition to these phases a tiny crystal of fluorite (70 nm) was found embedded in the matrix (see SP2). EELS analysis indicates the presence of Ca and F (with contribution of C and O from the surrounding matrix and the diffraction data fits fluorite structure (Table 3). Fluorite is a rare mineral in diamond (Gorshkov et al., 1997a,b; Titkov et al., 2006). Unlike other cavities, no crystalline carbonate phase was detected.

The groundmass is amorphous and heterogeneous in composition. It has a spongy structure that is characteristic of quenched material. It is rich in carbon and oxygen and variably enriched in Al and Si. Traces of Fe, K and Ca are also observed. Elemental mapping of the cavity reveals an Al:Si ratio of 2.4:1 (by weight, Table 2).

4.1.2. Microinclusions in diamond KFF-165

Seven HDF-bearing microinclusions were detected in the two foils extracted from this diamond (See SP3). Their size varies between 75 and 1400 nm. The microinclusions are rich in K and Cl (Na could not be analyzed due to the overlap of the Ga–L and Na–K peaks). In most cases the halides are crystalline and surrounded by amorphous material that contains mainly K, Si, Fe, Ca, Ba and P. In some cases the presence of apatite and carbonate is inferred from the chemical analyses but these phases are over- or under-lain by other material. In other cases the microinclusions contain only amorphous material with variable amount of the above mentioned elements and high contents of Cl and K. These compositions are in accordance with the K- and Cl-rich microinclusions that were analysed in the same diamond using EPMA (Izraeli et al., 2001) and are similar to that observed using TEM in a saline-HDF bearing diamond from Canada (Klein-BenDavid et al., 2006). However, while the inclusions in the Canadian diamond were mostly crystalline, in diamond KFF-165 they are dominated by amorphous material.

4.2. Diamonds from Yubileinaya (Yakutia, Sibiria)

Cavities were detected in two diamonds from the Yubileinaya mine, Yakutia, Siberia, UB 5–41 and UB 3105. Carbonatitic HDF and S–Fe–Ni bearing microinclusions were previously reported in diamond UB 5–41 (Klein-BenDavid et al., 2003; Logvinova et al., 2003). No microinclusions were detected using EPMA and neither water nor carbonate was detected by FTIR in diamond UB 3105. Larger inclusions of sulphides, chromite and Mg–Fe-silicates were found in its centre.

Four foils were cut from diamond UB 5–41, two of which contain large cavities. The cavity in foil #455 was briefly reported by Klein-BenDavid et al. (2006) and will be discussed here in details. Two foils were extracted from the inclusion-rich area in the centre of diamond UB 3105 and each carried a cavity. No microinclusions were detected in the foils.

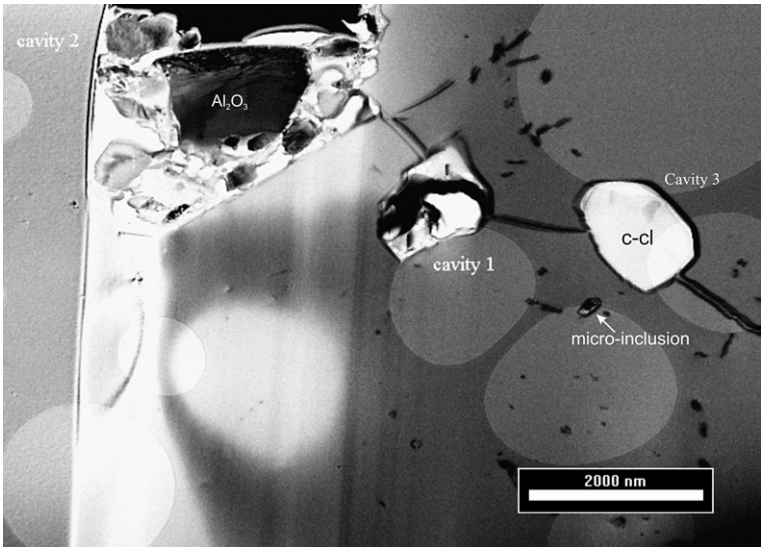

Fig. 4. Scanning transmission electron microscope (STEM) image showing three cavities aligned along a healed crack (foil #731, diamond UB-541). Also marked is a HDF-bearing microinclusion located near the line of cavities, the microinclusion preceded the dissolution event.

4.2.1. Cavities in foil #731, diamond UB 5–41

Three large cavities (1.5 to 4.5 μm in diameter) are aligned along a healed crack (Fig. 4) and were probably connected before healing. Cavity 1 contains heterogeneous amorphous material, rich in carbon and oxygen and enriched in Si, Al and Ca at various levels in the different zones. Phosphorous, S, Cl and Fe were identified in low abundances. Cavity 2 is the largest in this foil (only part of it is present in Fig. 4). It contains Ca-carbonate and Ca–Mg carbonate crystals as well as one large corroded corundum crystal. The crystals are embedded in a spongy amorphous matrix, rich in C, O, Si, Al, Fe and Ca and contain small amounts of P, S, Cl and K. A vacant space in the cavity was probably filled with fluid prior to foil extraction. EELS reveals the presence of nitrogen and indicates that the carbon is amorphous (e.g. Fig. 6a). The EEL spectra carbon K-edge has characteristic shapes for amorphous carbon, graphite or diamond. Both amorphous carbon and graphite display a pre-peak assigned to the π-electrons, which are absent in diamond. The round shape of the most prominent C-K edge in the present spectrum lacks the fine structure displayed by graphite and is characteristic of amorphous carbon. The Cu-support grid is coated with a film of amorphous carbon and could, in principle contribute to the spectrum. However, care was taken to analyze over a hole in the carbon grid.

The third cavity contains an amorphous phase, rich in carbon and chlorine. It is important to note that the analyzed section is only a part of a larger cavity that may

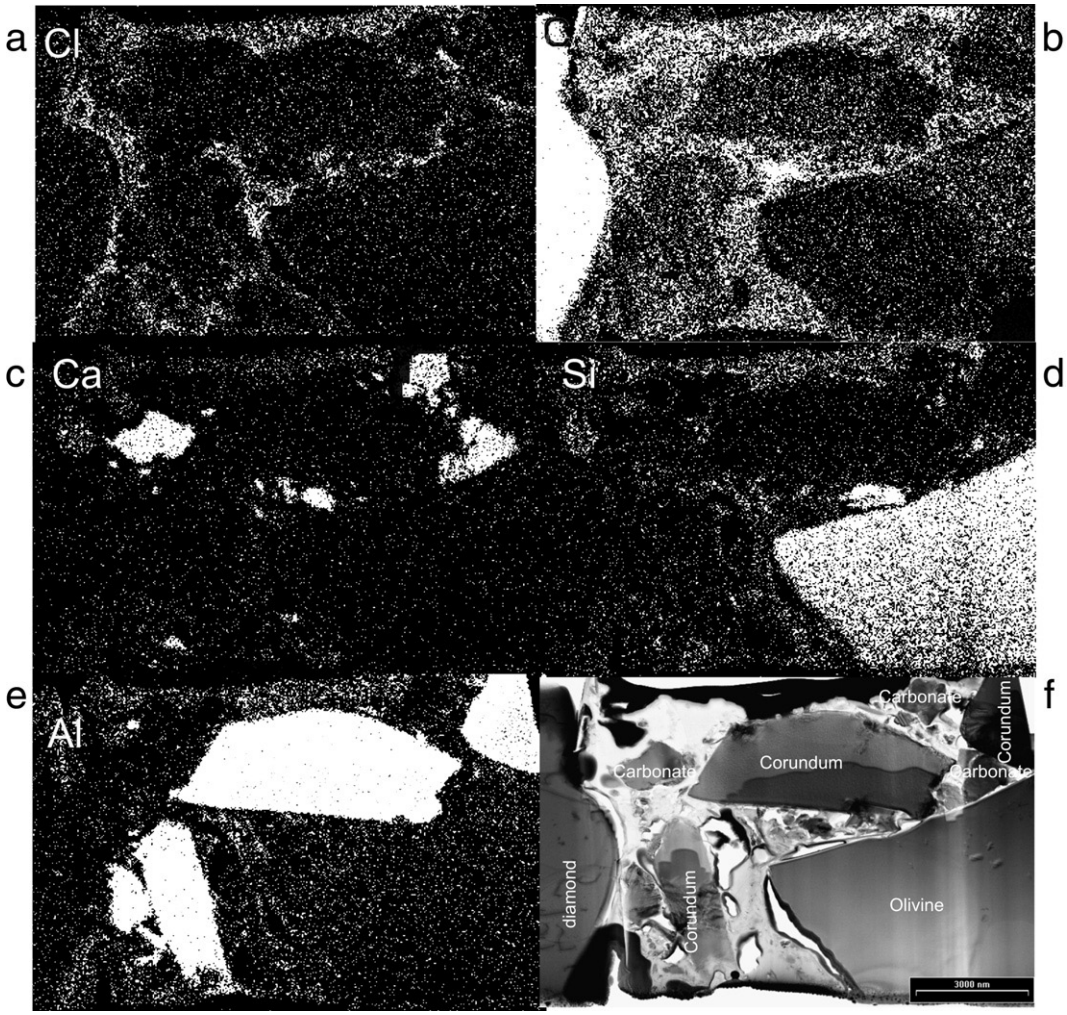

Fig. 5. Cavity in foil #543 from diamond UB 3105. (a–e) element maps. (a) and (b) indicate that the amorphous filling of the cavity is rich in C and Cl and reveal the spongy texture. (c) Ca-carbonate grains in the cavity. (d) Olivine grain (e) Corundum grains; all crystalline grains show resorption features. (f) STEM image. Voids in the filling were probably filled with a volatile phase prior to cavity rupture.

have contained more material. The enrichment in Cl is not consistent with the composition of the carbonatitic microinclusions of this diamond.

4.2.2. Cavities in foil #455, diamond UB 5–41

Three cavities (3.0, 0.68 and 0.75 μm in diameter) were exposed in this foil. We have investigated only the large cavity (see SP4). The cavity contains mostly spongy amorphous filling, rich in C and O and vacant spaces that were probably filled with a fluid prior to the foil extraction. A long acquisition time elemental map of a large part of the cavity indicates the heterogeneity of the material revealing zones that are variably rich in Al, Si and Ca with lesser amounts of Cl, K, Ti and Fe. EEL spectra acquired from both Al-rich and Ca-rich zones indicated that Al is bonded to oxygen and Ca to carbonate (SP5). The O–K edge observed in the EELS spectra shows a pre-edge at about 532 eV (SP5b) that is indicative of the presence of OH (Wirth, 1997) in the amorphous matrix.

Small crystals (10–200 nm) are embedded in the matrix (SP6a); the composition of the largest of them can be interpreted as carbonates, Al-oxide and a single ilmenite crystal.

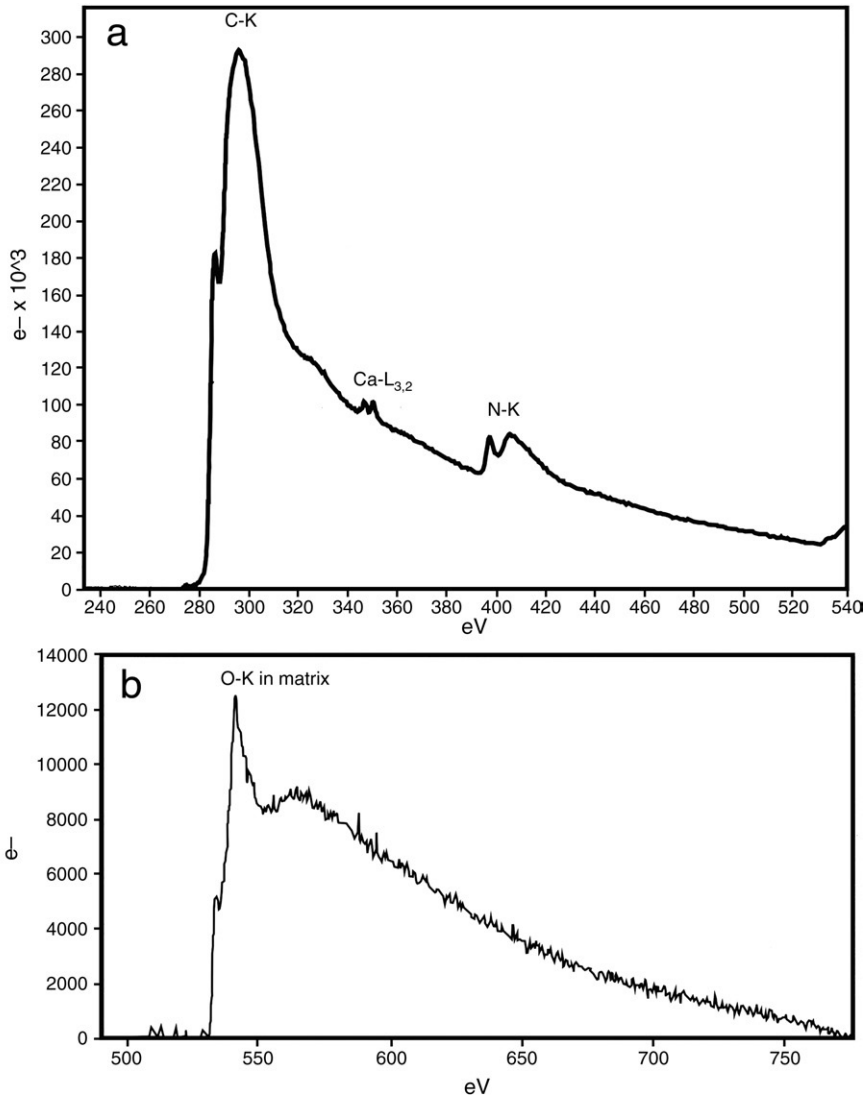

Fig. 6. (a) EEL spectrum of the amorphous matrix in the cavity in foil #543 of diamond UB 3105. The C–K edge structure is typical to amorphous carbon. N is abundant in the matrix (N–K edge), and Ca–$L_{3,2}$ edge is also visible in the spectrum. (b) The structure of the O–K edge in the matrix is similar to that of OH, indicating that water was probably an important component in the material trapped in the cavity. See text for details.

The interface between diamond and the cavity is uneven and has saw-tooth shape, suggesting diamond dissolution (e.g. SP6b).

4.2.3. Microinclusions in diamond UB 5–41

Ten microinclusions were detected in the four foils extracted from this diamond. They range in size between 50 and 700 nm and contain both amorphous and crystalline phases. The crystalline phases are commonly found in the larger inclusions. The most common crystals are Mg–Ca–Fe carbonates. Diffraction patterns taken from some of these crystals indicate aragonite structure (Table 3). We also identified a Mg–Fe silicate with a structure similar to that of serpentine (Table 3), a K–Cl halide and possibly apatite (mixed analysis). The amorphous material is commonly heterogeneous, rich in Mg and Ca, and also contains Fe, Si, P, K, Ba and Cl. This composition is in general agreement with the EPMA analyses of the microinclusions in that diamond (Klein-BenDavid et al., 2003 and Klein-BenDavid et al. in prep).

4.2.4. Cavities in foil #543, diamond UB 3105

The foil contains one large cavity (9 μm, Fig. 5f). The cavity includes crystalline aluminium-oxide (corundum, Fig. 5e), olivine (Fig. 5d) and carbonate phases (Fig. 5c) embedded in an amorphous matrix (Table 2). The amorphous matrix is rich in C and O as well as Ca and Cl; other elements such as Mg, Al, Si, P, S and Fe are present in low amounts (Fig. 5a and b). EEL spectra indicate that the carbon is amorphous and display high N contents (Fig. 6a). The O–K edge shows a pre-edge at about 532 eV (Fig. 6b) that is indicative for the presence of OH (Wirth, 1997). All crystalline phases show some resorption features. The carbonate crystals show re-growth of late polycrystalline carbonate on the top of the resorbed edge (SP6c). The diamond margins are uneven with a saw-tooth shape (SP6b).

4.2.5. Cavities in foil #550, diamond UB 3105

A single large cavity (~10 μm) includes aluminium-oxide (corundum) and quartz (see SP7) as well as carbonate crystals that present resorption along their edges. Nano-crystals (<10 nm) containing Ca and S were also found. All crystals are embedded in the amorphous matrix that contains mainly C, O and Cl with small amounts of Ca, S, Fe and Ni. Nitrogen was observed in the EELS spectra (e.g. Fig. 6a). Large voids in the cavity may have been filled with volatiles.

4.2.6. cavity in diamond CNG 2 (Congo)

Foil #1143 carries one large cavity (1 by 1.5 μm) that is located along a crack (SP8a). Its appearance is similar to the other cavities, with spongy amorphous matrix. However, the composition of the filling is considerably different to that found in the other diamonds. It is rich in amorphous carbon and N (e.g. Fig. 6a) with high concentrations of Si, Cl, K and Ca and trace amounts of Ni and Fe. Aluminum is not a major component of the matrix exposed in the foil. Dark field image shows minute crystals floating in the matrix (SP8b); the EELS analysis indicates that they are micro-diamonds.

4.2.7. Microinclusions in diamond CNG 2

Five microinclusions were detected in another foil cut from the same diamond. The inclusion filling is rich in Si with smaller and variable amounts of Al, P, Cl, K, Ca, Ti, Ba and Fe. It is distinct from that of the cavity by its high Al content and low levels of Cl. The filling is mostly amorphous, and has a spongy structure. The silica-rich composition is in accordance with the EPMA analysis of the microinclusions (Klein BenDavid — unpublished data) which indicates that the composition is close to the silicic-HDF end-member.

4.2.8. Cavities in foil #450, ON-DVK-294 (Diavik, Canada)

The two cavities in this foil were discussed in detail in Klein-BenDavid et al. (2006), thus only a brief description of the cavity filling will be given here. The foil exposes two elongated cavities 1×4 μm^2 and 2.5×8 μm^2. Most of the material in both cavities is amorphous, with only a few small crystals. Some of the area of the cavities is now empty. Cavity 1 is rich in Al and to a lesser degree in Si. Cavity 2 carries three distinct amorphous zones. The largest is rich in Al, with a few other elements; the second is rich in silica and also contains Al, Mg, Fe and K and the third is Ca-rich and contains minor phosphorus. Table 2 gives the overall composition of these cavities

5. Discussion

5.1. Micro inclusions

The overall composition of all the phases detected by TEM in single microinclusions is similar to that of the EPMA bulk analysis of individual microinclusions from the same diamonds (Izraeli et al., 2001; Klein-BenDavid et al., 2004, 2007; and Klein-BenDavid in preparation). In contrast to the crystalline nature of the secondary mineral assemblages found in cubic and coated diamonds from Canada (Klein-BenDavid et al., 2006) most of the microinclusions in this study have an amorphous, or

partly amorphous filling. Serpentine is found together with Ca-carbonate in the same single microinclusion in diamond UB 5–41. It may have crystallized as a secondary phase from the Mg-rich HDF. Alternatively serpentine may be a product of olivine–water reaction in the inclusion.

5.2. Cavities and their formation

Cavities in diamonds are found in various associations. They form cavity-rich layers in diamond ON-DVK-294; aligned in a row of cavities along a healed crack (Fig. 4) or found as isolated cavities within the diamond matrix. The cavities are anhedral in shape and their faces are commonly characterized by the uneven saw-tooth structures (SP6b).

The material in the cavities is mostly amorphous and spongy with open pores that probably contained volatiles prior to the extraction of the foil. Crystalline phases are also commonly embedded in the amorphous matrix.

Carbon is the main constituent of the amorphous matrix; nitrogen and water are also present, however these components could not be quantified. Amorphous zones rich in alumina, silica or calcium (the later mostly associated with carbonate) are also abundant and other elements are present in smaller amounts. Together, the amorphous and crystalline phases yield a bulk composition that is characterized by high carbon and alumina content. Such composition is distinct from that of the HDF trapped by the microinclusions. The composition of the cavity in diamond CNG 2 is different, but the distinction from that of the microinclusions is clear: chlorine content is high in the cavity whereas the microinclusions are Si-rich and Cl-depleted.

The difference in structure and composition between the cavities and the microinclusions even when they reside close to one another suggest that they represent two distinct generations. The association of the cavities with healed cracks suggests that they were formed and sealed after the entrapment of the HDFs in the microinclusions. The anhedral faces of the cavities and the saw-tooth shape suggest that the cavities may have formed during a dissolution event. Dissolution may also explain the high abundance of amorphous carbon in the matrix. In the case of diamond CNG 2, euhedral diamond nanocrystals are embedded in the carbon-rich matrix and were probably precipitated inside the cavity from the dissolution products. Similarly, the nitrogen in the matrix may also originate in the dissolved diamond. Nitrogen may play a role in the formation of the cavities. Preferential dissolution and cavity formation may be related to fine zoning in nitrogen content or aggregation. Such zoning in the distribution of nitrogen platelets was noted in KFF-166, a cloudy diamond from Koffiefontein (SP9). Dissolution may initiate at other defects, cracks or large inclusions as well and developed into surface pits or internal hollows. Renewed diamond growth may later seal the cavities.

The enrichment of the amorphous matrix in volatiles and in many minor elements (K, Fe, Ba, Mg, Cl, P, Ti and S) cannot be explained by the dissolution of microinclusions. Not only the compositions are different, but the amount of fluid in the few microinclusions that may have resided in the volume that now forms a cavity is trivial. A different fluid phase must have been present during the sealing of the cavities.

Micrometer-scale crystals were observed in four of the cavities, and include Al-oxide (corundum and κ-alumina), Ca- and Ca–Mg-carbonates, quartz, olivine and 6H-moissanite. Most crystals have anhedral shapes and show some resorption features. Al-oxides, quartz and carbonate are close in composition to the Al-, Si- or Ca-rich amorphous matrix. They may be related by amorphization of the former or crystallization of the letters. The large olivine crystal might have been trapped in an open pit at the diamond-host rock interface.

We propose that dissolution proceeded from the diamond surface along cracks or other imperfections and produced surface pits and internal hollows. The pits and hollows trapped some of the material dissolved from the diamond along with some mineral phases and fluid and were later sealed by renewed diamond growth.

The presence of both κ-alumina and moissanite in diamond KFF-165 is difficult to explain. κ-alumina is an orthorhombic metastable phase that has never been reported in nature. It is commonly produced by heat treatment of hydrated Al-minerals or by chemical vapor deposition. It preserves its structural identity only up to ~950 °C at surface pressure (Yourdshahyan et al., 1999).

Moissanite is a rare mineral inclusion in diamonds (e.g. Jaques et al., 1989; Moore and Gurney, 1989) and was also found together with heavy minerals separated from kimberlites (Mathez et al., 1995). Thermodynamic calculation in the Mg–Si–C–O system indicates that at mantle conditions SiC occur only at highly reducing conditions (4–7 log units below the iron-wustite (IW) buffer, Mathez et al., 1995). The above calculation was later confirmed by experiments (Ulmer et al., 1998). Arima et al. (2002) demonstrated that SiC fully reacts with carbonatitic melts to form diamond at 1500–1800 °C and 7.7 GPa. No SiC was found in the run products of these unbuffered experiments. However, equilibrium is not always maintained, or redox conditions may vary over short distances. Dobrzhinetskaya

and Green (2007) found SiC and diamond in experiments that were buffered to IW conditions, and noted that more reducing conditions may have been reached locally in parts of the capsule. Bulanova et al. (1998) found metalic iron, wustite and carbonate in a core of a diamond. Thus iron+wustite and carbonate+diamond, which should coexist only at different oxygen fugacity occurred in one place and were trapped in a single diamond.

We note that the presence of SiC is enigmatic, not only in the present case, but in the mantle in general. It should not co-exist with iron-bearing mantle minerals as it should reduce their iron to metal. It was suggested that it may exist locally in highly reduced micro-environments such as subducted biogenic material or serpentinized peridotite (Mathez et al., 1995). It is possible that the growth of diamond KFF-165 was initiated by penetration of carbonatitic fluids into such environment which led to reduction of the fluid, fast diamond formation and entrapment of the microinclusions. When this fluid was exhausted (no carbonates were detected in the cavity in this diamond), reduced conditions returned leading to partial dissolution of imperfections in the diamond and cavity formation. Moissanite, alumina and the resorbed diamond material were then trapped in the cavities. Later growth proceeds more slowly, and is based on carbon supply from further away or from dissolution of the imperfect diamonds formed in the first stage, cracks are healed, pits are sealed and the cavities are locked in the diamond. The role of the κ-alumina in this system is not clear, but in the context of the previous scenario, its formation may be related to the fast reactions between the oxidized fluids and the highly reduced silicate environment.

5.3. The composition of the cavity filling

All the analysed cavities with the exception of one are rich in alumina, silica and calcium, the later as Ca-carbonate. They are highly enriched in alumina and the alumina/silica ratio exceeds unity. This is true for cavities in both peridotitic and eclogitic diamonds.

Corundum and kyanite are rare mineral in eclogites and were reported as inclusions in eclogitic diamonds (Meyer and Giibelin, 1981; Harris, 1992; Sobolev et al., 1998; Sobolev et al., 1999; Hutchison et al., 2004) but never in peridotitc diamonds. Corundum together with micro-diamonds were found recently in volatile and carbonate-rich melt inclusion in garnet pyroxenite xenoliths from Hawaii as a part of an assemblage that represents a metasomatic melt (Wirth and Rocholl, 2003).

Enrichment in silica, alumina, calcium and sodium was recently noted in hydrous fluids in equilibrium with eclogites at 4–7 GPa and 700–1400 °C (Kessel et al., 2005). At 5 GPa, melting takes place between 1050 °C and 1100 °C. Near solidus fluids and melts are rich in silica and alumina, which together make ~80% of the solute, with CaO and Na_2O at around 5% each. The Al_2O_3/SiO_2 ratio increases with temperature between 900 and 1200 °C. This result is consistent with the observation of Manning (2006, 2007) for increasing solubility of alumina with pressure and temperature in the SiO_2–Al_2O_3–Na_2O–Cl system and of Aerts et al. (2007) in the K_2O–Al_2O_3–SiO_2–H_2O system.

As temperature rises towards the solidus the solute content of the fluids increases rapidly, while during melting (1050–1200 °C) the water content remains relatively constant and is ~20%. Thus, we expect that cooling of fluids would lead to the deposition of all elements and will be governed by silica. On the other hand the silica content in the melts remains constant while alumina increases, so cooling might lead to the precipitation of the aluminous assemblages.

Another important factor that cannot be evaluated from the data of Kessel et al. (2005) is the role of carbon. Hydrous fluids dissolve diamonds (Fedortchouk et al., 2007) and the dissolution leads to the formation of CO_2 or carbonate. The solubility of both silica and alumina decreases in the fluid/melt as it grows more carbonatitic. Thus, the interaction of hydrous fluids or near-solidus melts (or supercritical fluids at higher pressures) with diamonds may lead to diamond dissolution, carbonation of the fluid/melt and precipitation of non-carbonatitic components such as alumina and silica. Trapping of such fluids/melts together with excess alumina (as distinct mineral phases or as aluminous gel) may explain the chemical composition of the cavities.

The composition of hydrous fluids in equilibrium with peridotite is not known in such details, but alumina enrichment has been documented at grain boundaries in mantle xenoliths and may lead to formation of aluminous fluids in a peridotitic environment as well. Wirth (1996) and Franz and Wirth (1997) have reported Al-rich amorphous glasses (up to 40 wt.% Al_2O_3) along olivine and orthopyroxene grain boundary interfaces in mantle xenoliths. A similar phenomenon was observed in mantle xenoliths from Hawaii (Hiraga et al., 2003, 2004); however, the extent of the alumina enrichment at grain boundaries in this case was lower. Hiraga et al. (2004) suggest that during the infiltration of volatile rich fluids/melts through mantle rocks, selective dissolution would preferentially occur at grain edges and that these types of fluids will be out of equilibrium with the

crystalline grains and will be enriched in the elements that strongly partition to grain boundaries.

Diamond precipitation is governed by the presents of carbonate-rich high-density diamond-forming fluids that are trapped in the microinclusions, whereas the cavity formation occur in the presence of the fluid phase that is less common in the diamond source region. The HDF diamond forming fluids are related to carbonate enrichment in the mantle and may have a genetic relationship to kimberlitic melts, whereas the cavities represent less common events where corrosive fluids are introduced and lead to diamond dissolution.

In summary, we propose that micrometer scale cavities in diamonds form during dissolution events induced by the introduction of oxidizing hydrous fluids into the diamond growth area.

Diamonds commonly dissolve in hydrous fluids (Fedortchouk et al., 2007). Enrichment in silica, alumina calcium and sodium is documented in hydrous fluids that are in equilibrium with eclogites at diamond forming conditions (Kessel et al., 2005), and this enrichment consistent with the increased solubility of alumina with increased pressure and temperature in the SiO_2–Al_2O_3–Na_2O–Cl system (Manning, 2006, 2007). Alumina and incompatible element enrichment is also observed at grain boundaries in peridotites and may be enriched in fluids/melts that selectively dissolve the grain edges.

Diamond dissolution forms oxidized carbon species and may affect the solubility of silica and alumina in the dissolving agent. Thus, the interaction of hydrous fluids/melts with diamonds should lead to precipitation of non-carbonatitic components such as alumina and silica. Trapping of such fluids/melts together with the precipitated alumina may explain the chemical composition of the cavities.

Diamond forming fluids that are trapped as micro-inclusions in fibrous diamonds are the dominant fluid component in the diamond growth area. Corrosive hydrous fluids are less common and appear as short, discrete events, followed by the return of the common HDFs and continued diamond precipitation.

Acknowledgments

We thank Larissa Dobrzhinetskaya and an anonymous reviewer for constructive reviews, Victoria Martin for her help in editing, Diavik Mining Corporation, Nik Sobolev and Alla Logvinova for contributing the diamonds. Research was supported by the US–Israel Binational Science Foundation (BSF 2004161), a Minerva short term research grant and a Marie Currie 6pf operation.

Appendix A. Supplementary data

Supplementary data associated with this article can be found, in the online version, at doi:10.1016/j.epsl.2007.09.004.

References

Aerts, M., Hack, A.C., Thompson, A.B., Ulmer, P., 2007. Mineral-buffered fluid compositions in K_2O–Al_2O_3–SiO_2–H_2O to 2.0 GPa and 800 °C as measured by the diamond-trap method. Geophys. Res. Abstr. 9, 04167.

Arima, M., 1998. Experimental study of growth and resorption of diamond in kimberlitic melts at high pressures and temperatures. Extended abstracts, 7th International Kimberlite Conference, Cape Town, pp. 32–34.

Arima, M., Kozai, Y., Akaishi, M., 2002. Diamond nucleation and growth by reduction of carbonate melts under high-pressure and high-temperature conditions. Geology 30, 691–694.

Bulanova, G.P., 1995. The formation of diamond. J. Geochem. Explor. 53, 1–23.

Bulanova, G.P., Griffin, W.L., Ryan, C.G., 1998. Nucleation environment of diamonds from Yakutian kimberlites. Mineral. Mag. 62, 409–419.

Burgess, R., Layzelle, E., Turner, G., Harris, J.W., 2002. Constraints on the age and halogen composition of mantle fluids in Siberian coated diamonds. Earth Planet. Sci. Lett. 197, 193–203.

Dobrzhinetskaya, L.F., Green, H.W., 2007. Diamond synthesis from graphite in the presence of water and SiO_2: Implications for diamond formation in quartzites from Kazakhstan. Int. Geol. Rev. 49, 389–400.

Egerton, R.F., 1996. Electron energy-loss spectroscopy in the electron microscope, second edition. Plenum Press.

Fedortchouk, Y., Canil, D., Carlson, J.A., 2005. Dissolution forms in Lac de Gras diamonds and their relationship to the temperature and redox state of kimberlite magma. Contrib. Mineral. Petrol. 150, 54–69.

Fedortchouk, Y., Canil, D., Semenets, E., 2007. Mechanisms of diamond oxidation and their bearing on the fluid composition in kimberlite magmas. Am. Mineral. 92, 1200–1212.

Franz, L., Wirth, R., 1997. Thin intergranular melt films and melt pockets in spinel peridotite xenoliths from the Rhone area (Germany): early stage of melt generation by grain boundary melting. Contrib. Mineral. Petrol. 129, 268–283.

Gorshkov, A.I., Bao, Y.N., Bershov, L.V., Ryabchikov, I.D., Sivtsov, A.V., Lapina, M.I., 1997a. Inclusions in diamond from the Liaoning deposit (China) and their genetic meaning. Geokhimiya 58–65.

Gorshkov, A.I., Bao, Y.N., Bershov, L.V., Ryabchikov, I.D., Sivtsov, A.V., Lapina, M.I., 1997b. Inclusions of native metals and other minerals in diamond from Kimberlite pipe 50, Liaoning, China. Geokhimiya 794–804.

Guthrie, G.D., Veblen, D.R., Navon, O., Rossman, G.R., 1991. Submicrometer fluid inclusions in turbid-diamond coats. Earth Planet. Sci. Lett. 105, 1–12.

Harris, J., 1992. Diamond Geology. In: Field, J. (Ed.), The Properties of Natural and Synthetic Diamonds, vol. 58A(A–K), pp. 384–385.

Hiraga, T., Anderson, I.M., Kohlstedt, D.L., 2003. Chemistry of grain boundaries in mantle rocks. Am. Mineral. 88, 1015–1019.

Hiraga, T., Anderson, I.M., Kohlstedt, D.L., 2004. Grain boundaries as reservoirs of incompatible elements in the Earth's mantle. Nature 427, 699–703.

Hutchison, M.T., Nixon, P.H., Harley, S.L., 2004. Corundum inclusions in diamonds — discriminatory criteria and a corundum compositional dataset. Lithos 77, 273–286.

Izraeli, E.S., Harris, J.W., Navon, O., 2001. Brine inclusions in diamonds: a new upper mantle fluid. Earth Planet. Sci. Lett. 187, 323–332.

Izraeli, E.S., Harris, J.W., Navon, O., 2004. Fluid and mineral inclusions in cloudy diamonds from Koffiefontein, South Africa. Geochim. Cosmochim. Acta. 68, 2561–2575.

Jaques, A.L., Hall, A.E., Sheraton, J.W., Smith, J.B., Sun, S.S., Drew, R.M., Foudoulis, C., Ellingsen, K., 1989. Composition of crystalline inclusions and C-isotope composition of Argyle and Ellendale diamonds. In: Ross, J., Jaques, A.L., Ferguson, J., Green, D.H., O'reilly, S.Y., Danchin, R.V., Janse, A.J.A. (Eds.), Kimberlite and Related Rocks, Volume 2: Their Mantle/Crust Setting, Diamonds and Diamond Exploration. Geological Society of Australia Special Publication, vol. 14. Blackwell Scientific, pp. 966–989.

Kanda, H., Yamaoka, S., Setaka, N., Komatsu, H., 1977. Etching of diamond octahedrons by high pressure water. J. Cryst. Growth 38, 1–7.

Kessel, R., Ulmer, P., Pettke, T., Schmidt, M.W., Thompson, A.B., 2005. The water–basalt system at 4 to 6 GPa: Phase relations and second critical endpoint in a K-free eclogite at 700 to 1400 °C. Earth Planet. Sci. Lett. 237, 873–892.

Khokhryakov, A.F., Pal'yanov, Y.N., 2007. The evolution of diamond morphology in the process of dissolution: Experimental data. Am. Mineral. 92, 909–917.

Khokhryakov, A.F., Pal'yanov, Y.N., Sobolev, N.V., 2001. Evolution of crystal morphology of natural diamond in dissolution processes: Experimental data. Dokl. Earth Sci. 381, 884–888.

Khokhryakov, A.F., Pal'yanov, Y.N., Sobolev, N.V., 2002. Crystal morphology as an indicator of redox conditions of natural diamond dissolution at the mantle PT parameters. Dokl. Earth Sci. 385, 534–537.

Klein-BenDavid, O., Logvinova, A.M., Izraeli, E., Sobolev, N.V., Navon, O., 2003. Sulfide melt inclusions in Yubileinayan (Yakutia) diamonds. 8th international kimberlite conference, Extended abstracts, Victoria, Canada, FLA_0111.

Klein-BenDavid, O., Izraeli, E.S., Hauri, E., Navon, O., 2004. Mantle fluid evolution — a tale of one diamond. Lithos 77, 243–253.

Klein-BenDavid, O., Wirth, R., Navon, O., 2006. TEM imaging and analysis of microinclusions in diamonds: a close look at diamond-growing fluids. Am. Mineral. 91, 353–365.

Klein-BenDavid, O., Izraeli, E.S., Hauri, E., Navon, O., 2007. Fluid inclusions in diamonds from the Diavik mine, Canada and the evolution of diamond-forming fluids. Geochim. Cosmochim. Acta 71, 723–744.

Klein-BenDavid, O., Logvinova, A., Sobolev, N.V., Schrauder, M., Spetius, Z., Hauri, E., Navon, O., in preparation. Yakutian diamond-forming fluids — the evolution of carbonatitic high density fluids.

Kozai, Y., Arima, M., 2005. Experimental study on diamond dissolution in kimberlitic and lamproitic melts at 1300–1420 °C and 1 GPa with controlled oxygen partial pressure. Am. Mineral. 90, 1759–1766.

Lang, A.R., Walmsley, J.C., 1983. Apatite inclusions in natural diamond coat. Phys. Chem. Miner. 9, 6–8.

Logvinova, A.M., Klein-BenDavid, O., Izraeli, E.S., Navon, O., Sobolev, N.V., 2003. Micro-inclusions in fibrous diamonds from Yubilenaya kimberlite pipe (Yakutia). 8th international kimberlite conference, extended abstracts, FLA_0025.

Manning, C.E., 2006. Mobilizing aluminum in crustal and mantle fluids. J. Geochem. Explor. 89, 251–253.

Manning, C.E., 2007. Solubility of corundum+kyanite in H_2O at 700C and 10 kbar: evidence for Al–Si complexing at high pressure and temperature. Geofluids 7, 258–269.

Mathez, E.A., Fogel, R.A., Hutcheon, I.D., Marshintsev, V.K., 1995. Carbon isotopic composition and origin of SiC from kimberlites of Yakutia, Russia. Geochim. Cosmochim. Acta 59, 781–791.

McCallum, M.E., Huntley, P.M., Falk, R.W., Otter, M.L., 1994. Morphological, resorption and etch feature trends of diamonds from kimberlite populations within the Colorado–Wyoming State Line district, USA. Proceedings of the 5th International Kimberlite Conference, Rio de Janeiro, pp. 32–50.

Meyer, H.O.A., Giibelin, E., 1981. Ruby in diamond. Gems. Gemol. 17, 153–156.

Moore, R.O., Gurney, J.J.I., 1989. Mineral inclusions in diamond from the Monastery kimberlite, South Africa. In: Ross, J., Jaques, A.L., Ferguson, J., Green, D.H., O'reilly, S.Y., Danchin, R.V., Janse, A.J.A. (Eds.), Kimberlite and Related Rocks, Volume 2: Their Mantle/Crust Setting, Diamonds and Diamond Exploration. Geological Society of Australia Special Publication, vol. 14, pp. 1029–1041.

Navon, O., 1991. High internal-pressures in diamond fluid inclusions determined by infrared-absorption. Nature 353, 746–748.

Pal'yanov, Y.N., Khokhryakov, A.F., Borzdov, Y.M., Sokol, A.G., 1995. Diamond morphology in growth and dissolution precesses. 6th International Kimberlite Conference, extended abstract, pp. 415–417.

Pearson, D.G., Shirey, S.B., Harris, J.W., Carlson, R.W., 1998. Sulphide inclusions in diamonds from the Koffiefontein kimberlite, S Africa: constraints on diamond age and mantle Re–Os systematics. Earth Planet. Sci. Lett. 160, 311–326.

Robinson, D.N., 1978. Characteristics of natural diamond and their interpretation. Miner. Sci. Eng. 10, 55–72.

Robinson, D.N., Scott, J.A., Niekerk, A.V., Anderson, V.G., 1989. The sequencef events reflected in the diamonds of some southern African kimberlites. In: Ross, J., Jaques, A.L., Ferguson, J., Green, D.H., O'reilly, S.Y., Danchin, R.V., Janse, A.J.A. (Eds.), Kimberlite and Related Rocks, Volume 2: Their Mantle/Crust Setting, Diamonds and Diamond Exploration. Geological Society of Australia Special Publication, vol. 10, pp. 990–1000.

Schulze, D.J., Harte, B., Valley, J.W., Brenan, J.M., Channer, D.M.D., 2003. Extreme crustal oxygen isotope signatures preserved in coesite in diamond. Nature 423, 68–70.

Sobolev, N.V., Yefimova, E.S., Channer, D.M.D., Anderson, P.F.N., Barron, K.M., 1998. Unusual upper mantle beneath Guaniamo, Guyana shield, Venezuela: Evidence from diamond inclusions. Geology 26, 971–974.

Sobolev, N.V., Sobolev, V.N., Snyder, G.A., Yefimova, E.S., Taylor, L.A., 1999. Significance of eclogitic and related parageneses of natural diamonds. Int. Geol. Rev. 41, 129–140.

Sunagawa, I., 1984. Morphology of natural and synthetic diamond crystals. In: Sunagawa, I. (Ed.), Materials Science of the Earth's interior. Terra Scientific, pp. 303–330.

Sunagawa, I., 1990. Growth and Morphology of Diamond Crystals under Stable and Metastable Conditions. J. Cryst. Growth 99, 1156–1161.

Titkov, S.V., Gorshkov, A.I., Zudin, N.G., Ryabchikov, I.D., Magazina, L.O., Sivtsov, A.V., 2006. Microinclusions in dark gray diamond crystals of octahedral habit from Yakutian kimberlites. Geochem. Int. 44, 1121–1128.

Tomlinson, E.L., Jones, A.P., Harris, J.W., 2006. Co-existing fluid and silicate inclusions in mantle diamond. Earth Planet. Sci. Lett. 250, 581–595.

Ulmer, G.C., Grandstaff, D.E., Woermann, E., Gobbels, M., Schonitz, M., Woodland, A.B., 1998. The redox stability of moissanite

(SiC) compared with metal-metal oxide buffers at 1773 K and at pressures up to 90 kbar. Neues Jahrb. Mineral. Abh. 172, 279–307.

Walmsley, J.C., Lang, A.R., 1992a. On submicrometer inclusions in diamond coat — Crystallography and composition of ankerites and related rhombohedral carbonates. Mineral. Mag. 56, 533–543.

Walmsley, J.C., Lang, A.R., 1992b. Oriented biotite inclusions in diamond coat. Mineral. Mag. 56, 108–111.

Wirth, R., 1996. Thin amorphous films (1–2 nm) at olivine grain boundaries in mantle xenoliths from San Carlos, Arizona. Contrib. Mineral. Petrol. 124, 44–54.

Wirth, R., 1997. Water in minerals detectable by electron energy-loss spectroscopy EELS. Phys. Chem. Miner. 24, 561–568.

Wirth, R., 2004. Focused Ion Beam (FIB): A novel technology for advanced application of micro- and nanoanalysis in geosciences and applied mineralogy. Eur. J. Mineral. 16, 863–876.

Wirth, R., Rocholl, A., 2003. Nanocrystalline diamond from the Earth's mantle underneath Hawaii. Earth Planet. Sci. Lett. 211, 357–369.

Yourdshahyan, Y., Ruberto, C., Halvarsson, M., Bengtsson, L., Langer, V., Lundqvist, B.I., Ruppi, S., Rolander, U., 1999. Theoretical structure determination of a complex material: kappa-Al_2O_3. J. Am. Ceram. Soc. 82, 1365–1380.

Zedgenizov, D.A., Harte, B., Shatsky, V.S., Politov, A.A., Rylov, G.M., Sobolev, N.V., 2006. Directional chemical variations in diamonds showing octahedral following cuboid growth. Contrib. Mineral. Petrol. 151, 45–57.